Pd-doped In$_2$O$_3$ nanocomposites for the photocatalytic degradation of atrazine

E.S. Aazam[a], R.M. Mohamed[a,b,*], T.M. Hassan[a]

[a]*Chemistry Department, Faculty of Science, King Abdulaziz University, Jeddah 21589, P.O. Box 80203, Saudi Arabia,*
emails: redama123@yahoo.com (R.M. Mohamed), elhamaazam@gmail.com (E.S. Aazam), jodabdullah@hotmail.com (T.M. Hassan)
[b]*Nanostructured Material Division Advanced Materials Department, Central Metallurgical R&D Institute, Helwan,*
11421 Cairo, Egypt

ABSTRACT

Palladium-doped indium oxide nanocomposites were prepared by a sol-gel method using tetrabutylammonium hydroxide as a surfactant. Many tools were used to describe the synthesized nanocomposites. The X-ray diffraction results reveal that only a single phase for In$_2$O$_3$ is observed for undoped or doped In$_2$O$_3$ samples. There are no characteristic peaks for palladium or palladium oxide because the dispersion of palladium above the indium oxide surface is high. XPS results reveal that the state of palladium is metallic. The values of band gap energy for indium oxide, 0.1 wt% palladium-doped indium oxide, 0.2 wt % palladium-doped indium oxide, 0.3 wt% palladium-doped indium oxide and 0.4 wt% palladium-doped indium oxide samples are 2.68, 2.51, 2.41, 2.32 and 2.25 eV, respectively. Therefore, the band gap energy of In$_2$O$_3$ can be controlled by controlling the weight percentage of doped palladium. The photocatalytic performance of In$_2$O$_3$ and Pd-doped In$_2$O$_3$ nanocomposites was studied by measuring atrazine photocatalytic degradation under visible light. Parameters of photocatalytic reactions, such as palladium weight percentage and dose of 0.3 wt% palladium-doped indium oxide nanocomposites, were measured. The palladium-doped indium oxide nanocomposites had photocatalytic activity higher than that of In$_2$O$_3$ because the addition of Pd to In$_2$O$_3$ decreases the recombination rate of the electron–hole; furthermore, the absorption of In$_2$O$_3$ was shifted to a high wavelength.

Keywords: In$_2$O$_3$; Pd; Atrazine degradation; Visible photocatalyst

1. Introduction

In recent years, the release of industrial wastewater is considered the most serious health concern in many countries all over the world [1]. Many resources are responsible for organic pollutants, and pesticides have been found in water, with special concentrations in wastewater. More particularly, pesticides have high toxicity and have a direct effect on popular health matters because of their high environmental threat [2,3]. Pesticides are categorized as insecticides, fungicides, herbicides and bactericides [4]. Atrazine is one of the most vital and familiar pesticides [5]. The most familiar pesticides also comprise cypermethrin, chlorothalonil, chlorpyrifos and methamidophos [6]. Many studies have reported that surface and underground water are highly contaminated with pesticides [7–9]; further contamination occurs in tap and fresh water resources with concentrations of approximately 500 ppm [10]. Photocatalysis, adsorption, membrane filtration, oxidation biosorption and other techniques have been reported as promising methods for wastewater remediation [11–15], and photocatalysis has been reported as a superior technique due to its high photocatalytic stability and activity as well as its easy self-regeneration ability [16,17]. Nanotechnology manufacture is an important type

* Corresponding author.

of modern science that addresses the design, fabrication and application of tiny molecules in the range of nanometers [18–20]. Titanium dioxide nanoparticles have been widely utilized as a photocatalyst; they are notably non-toxic, commercially available, inexpensive and demonstrate reasonable photochemical stability [21–24]. Furthermore, titanium dioxide has a higher thermal stability and photocatalytic activity as well as acceptable redox properties compared with other photocatalysts; thus, titanium dioxide is classified as one of the most desirable photocatalysts for wastewater treatment [21,22]. The most common crystal phases for titanium dioxide are brookite, anatase and rutile. The anatase phase is the major effective and efficient phase [25]. In the open literature, prepared titanium dioxide nanoparticles have been examined and illustrated as effective photocatalysts in pesticide degradation [26–28]. More particularly, titanium dioxide has shown higher activity when reacted under UV light, where 3%–5% of the solar spectrum was appointed due to its large band gap and reported as E_g = 3.2 eV. Therefore, working groups are attempting to design and estimate a formula to reduce the band gap; hence, the produced material would be more efficient in artificial or natural sunlight [14]. On the other hand, significant interest has been generated in studying In_2O_3 as a special substance of variable applications. These applications include optical fiber behavior, photoanodes, scintillators and laser hosts [26,28–30]. In_2O_3 has been examined in the literature as an excellent photocatalyst for the photodegradation of numerous organic pollutants in the presence of UV radiation [26–31]. Furthermore, metallic dopants, morphologies and surface structures have been used to estimate and control the photocatalytic activity execution of titanium dioxide, as previously mentioned [32–34]. The present work is aimed to synthesize a new Pd-doped In_2O_3 nanocomposite via the sol-gel technique. In the operational process, tetrabutylammonium hydroxide (TBAOH) was consumed for the synthesis of In_2O_3 for the first time as a matrix. The newly designed materials will also be applied for atrazine photocatalytic degradation.

2. Experimental methods

2.1. Preparation of photocatalysts

Three grams of TBAOH was dissolved under magnetic stirring in bi-distilled water (20 mL). Then, 0.05 M of indium nitrate was added to a TBAOH solution dropwise and stirred for 60 min to form mixture A. The required amount of palladium chloride, which needed to be prepared at different wt% of palladium to indium oxide, for example, 0.1, 0.2, 0.3 and 0.4 wt%, were dissolved under magnetic stirring in bi-distilled water (50 mL) to form mixture B. Mixture A was added in a dropwise manner to mixture B, and the resulting mixture was left to form gel. The produced gel was dried in an oven at 473 K. The produced materials were calcined at 773 K for 2 h. The nanocomposites were calcined under a flow of hydrogen gas for 2 h at 423 K. To prepare indium oxide, the above method was repeated without the use of palladium chloride.

2.2. Photocatalysts characterization

The morphological, chemical and physical properties of In_2O_3 and Pd-doped In_2O_3 nanocomposites were investigated using different characterization techniques. Transmission electron microscopy (TEM) was used to investigate the nanostructure morphology and sample dimensions using a JEOL-JEM-1230. The texture properties and surface area analysis were performed using N_2 adsorption measurements with a Nova 2000 series Chromatech apparatus at 77 K after degassing the samples for 2 h at 373 K. Powder X-ray diffraction (XRD) was used to study the crystallinity of the samples using a Bruker axis D8 with Cu Kα radiation (λ = 1.540 Å) at room temperature. A UV–Vis–NIR spectrophotometer (V-570, Jasco, Japan) was used to determine the UV–Vis diffusion reflectance spectra (UV–Vis-DRS) to estimate the band gap performance over a range of 200–800 nm. A Shimadzu RF-5301 fluorescence spectrophotometer was used to determine the photoluminescence (PL) emission spectra.

2.3. Photocatalytic activity

Indium oxide and palladium-doped indium oxide were used to measure the degradation of atrazine using visible light. An annular batch reactor with a horizontal cylinder was used for the photocatalytic reaction. A 150-W blue fluorescent lamp with a maximum energy of 450 nm and a UV cut filter covering was used to irradiate the In_2O_3 and Pd-doped In_2O_3 nanocomposite photocatalysts, which were spread in 1,000 mL of atrazine solution with a 100-ppm atrazine concentration. The photocatalytic reactions were conducted at room temperature. Samples from the reaction mixture were taken at preset interval times to measure In_2O_3 and Pd-doped In_2O_3 nanocomposite photocatalytic activity. A high-pressure liquid chromatography LC 20 A with a C18 column UV detector (Shimadzu) was used to determine the concentration of atrazine remaining in the reaction mixture. The removal efficiency of atrazine was measured by adopting the following equation:

$$\text{\% Removal efficiency} = (C_o - C)/C_o \times 100 \qquad (1)$$

where C_o is the initial concentration of atrazine, and C is the remaining concentration of atrazine.

Ion chromatography (DX-300) with a CDM-II conductivity detector and a AS4A-SC column were used to measure chloride and nitrate ion concentrations. The gases obtained from the photocatalytic reaction were passed through a sodium hydroxide solution with a concentration of 0.2 M, and a barium nitrate solution was added to the obtained materials; the produced precipitate was identified by XRD.

3. Results and discussion

3.1. Photocatalyst characterizations

Fig. 1 shows the XRD patterns of In_2O_3 and Pd-doped In_2O_3 nanocomposites. The marks show that only a single phase for In_2O_3 is observed for undoped or doped In_2O_3 samples. Additionally, no characteristic peaks for palladium or palladium oxide due to the amount of palladium are found in the low detection limit of XRD, and the dispersion of palladium above the indium oxide surface is high. Moreover,
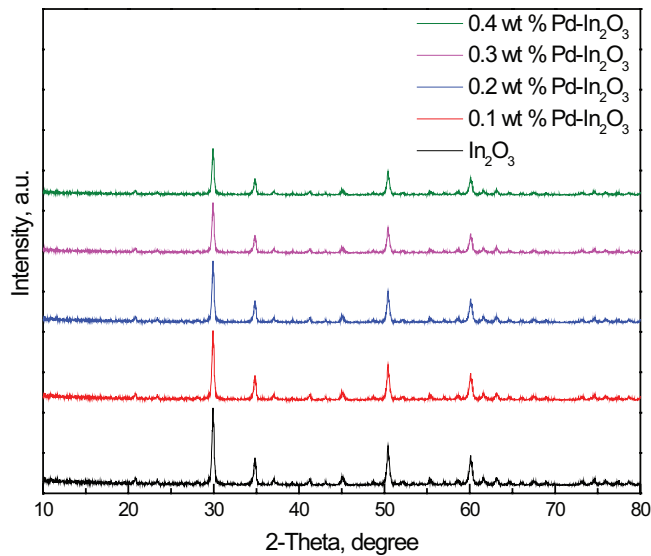
Fig. 1. XRD patterns of Indium oxide and palladium-doped indium oxide nanocomposites.

the heights of the indium oxide characteristic peaks are decreased by the palladium doping.

Fig. 2 shows the XPS spectra of 0.3 wt% palladium-doped indium oxide sample for In3d, O1s and Pd3d. The results of Fig. 2(A) revealed that the presence of two peaks at 444.6 and 452.2 eV for In3d confirm the presence of indium(III) [35]. The results of Fig. 2(B) revealed that the presence of one peak at 529.2 eV for O1s confirmed the presence of an O^{2-} ion [35]. Fig. 2(C) revealed that the presence of two peaks at 341.7 and 336.4 eV for Pd3d confirmed the presence of palladium metal. Therefore, the nanocomposite was composed of metallic palladium-doped In_2O_3 [35].

The TEM images of In_2O_3 and Pd-doped In_2O_3 nanocomposites are shown in Fig. 3. The marks verified that as the weight percent of doped palladium increased from 0 to 0.3 wt%, the dispersion increased, as shown in Figs. 3(A)–(D). However, with an increased weight percent of doped palladium above 0.3 wt%, the agglomeration of palladium also increased, as shown in Fig. 3(E). Therefore, the dispersion of palladium above the surface of In_2O_3 could be controlled by controlling the weight percentage of doped palladium.

Table 1 shows the BET surface area of In_2O_3 and Pd-In_2O_3 nanocomposites. Marks reveal that the surface area values are 30, 28, 24, 22 and 18 m^2/g for Indium oxide, 0.1 wt% palladium-doped indium oxide, 0.2 wt% palladium-doped indium oxide, 0.3 wt% palladium-doped indium oxide and 0.4 wt% palladium-doped indium oxide samples, respectively. Therefore, the addition of palladium blocked some pores of indium oxide and decreased its surface area.

The UV–Vis spectra of In_2O_3 and Pd-doped In_2O_3 nanocomposites are shown in Fig. 4. The marks revealed that as the weight percentage of doped palladium was increased from 0 to 0.4 wt%, the absorption edge of In_2O_3 was moved to a high wavelength. UV–Vis spectra were used to calculate band gap energy values for indium oxide, 0.1 wt% palladium-doped indium oxide, 0.2 wt% palladium-doped indium oxide, 0.3 wt% palladium-doped indium oxide and 0.4 wt% palladium-doped indium oxide of 2.68, 2.51, 2.41,
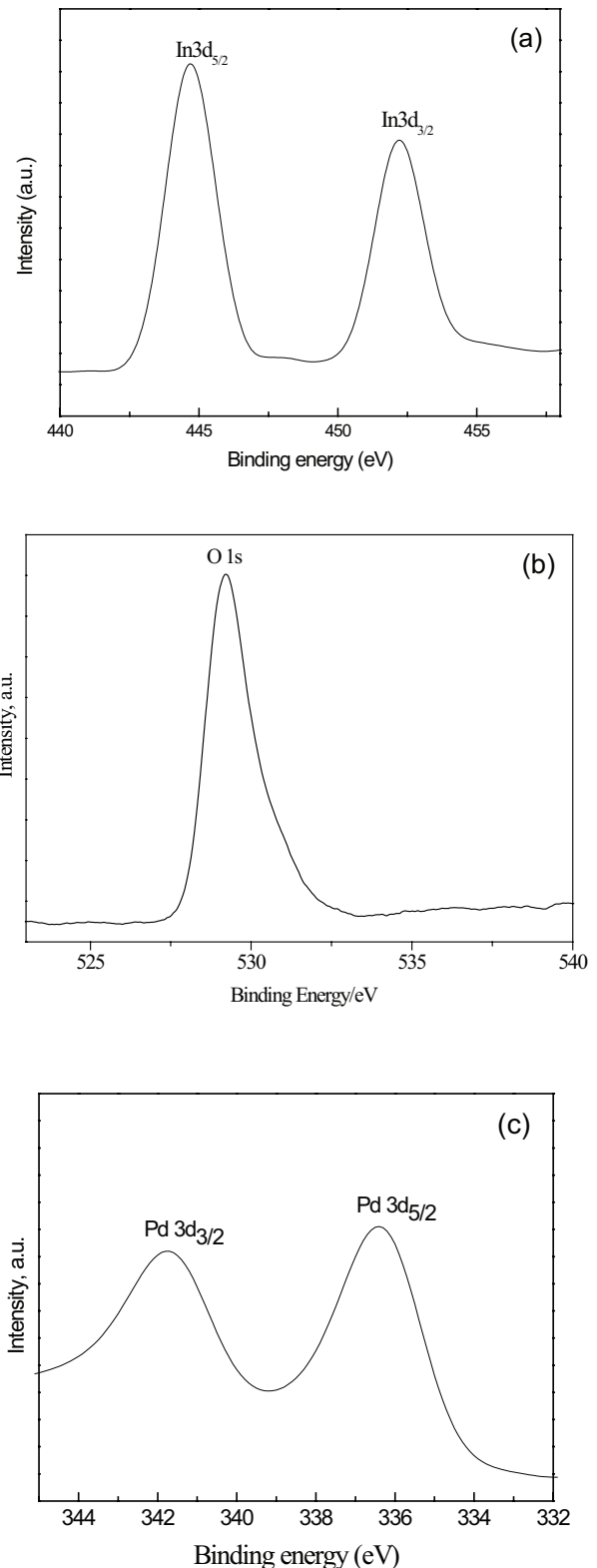

Fig. 2. XPS spectra of 0.3 wt% palladium-doped indium oxide sample, where (A) In3d; (B) O1s and (D) Pd3d.

2.32 and 2.25 eV, respectively. Therefore, the band gap energy of In_2O_3 could be controlled by the control weight percentage of doped palladium.
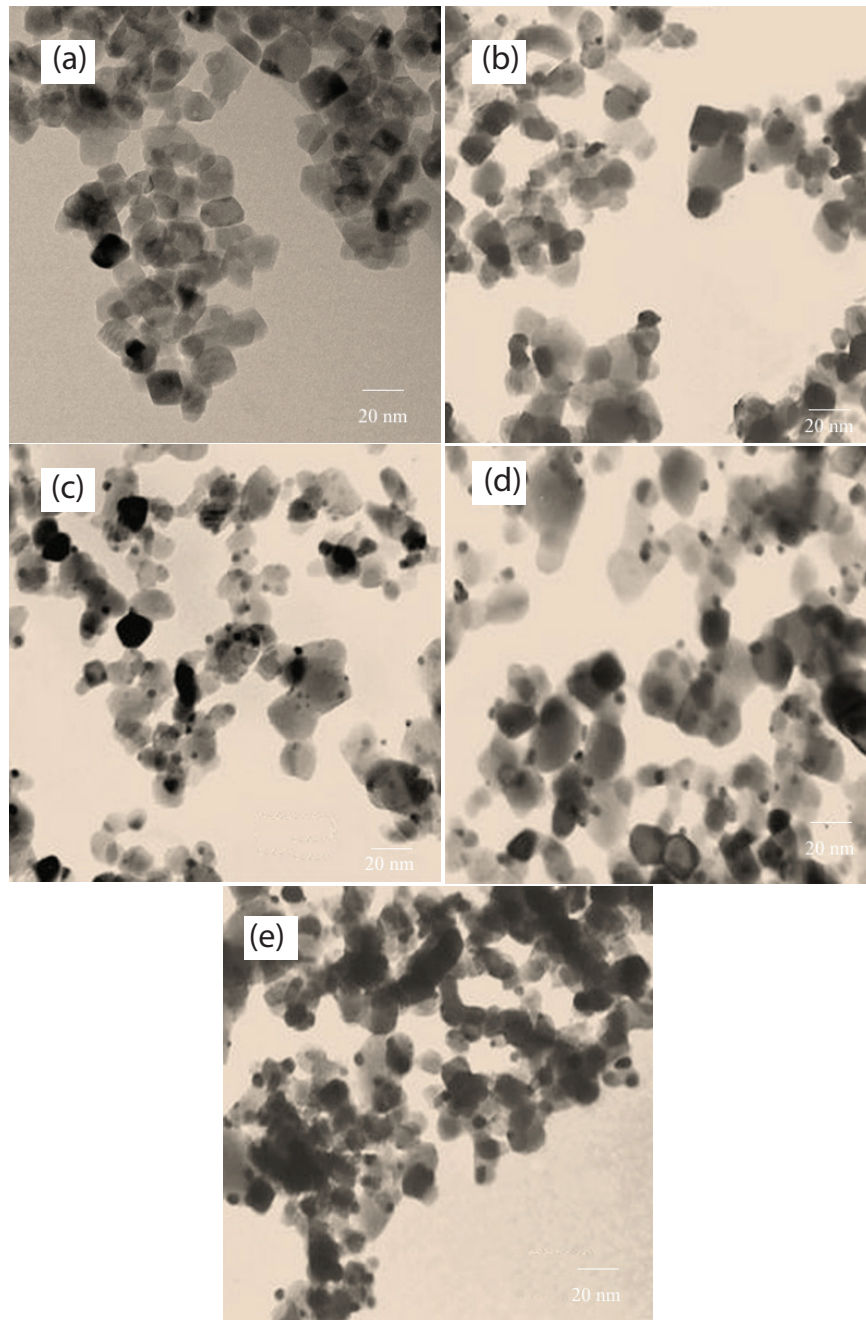
Fig. 3. TEM images of indium oxide and palladium-doped indium oxide nanocomposites, where (A) indium oxide; (B) 0.1 wt% palladium-doped indium oxide; (C) 0.2 wt% palladium-doped indium oxide; (D) 0.3 wt% palladium-doped indium oxide and (E) 0.4 wt% palladium-doped indium oxide samples.

Table 1
BET surface area of In_2O_3 and $Pd-In_2O_3$ nanocomposites

Samples	Surface area (m^2/g)
In_2O_3	30.0
0.1 wt% $Pd-In_2O_3$	28.0
0.2 wt% $Pd-In_2O_3$	24.0
0.3 wt% $Pd-In_2O_3$	22.0
0.4 wt% $Pd-In_2O_3$	18.0

The PL spectra of In_2O_3 and Pd-doped In_2O_3 nanocomposites are shown in Fig. 5. The marks reveal that as the weight percentage of doped palladium increased from 0 to 0.4 wt%, the peak intensity of PL of In_2O_3 decreased. Therefore, the addition of palladium to In_2O_3 increased the lifetime rate for electron–hole recombination and increased the photocatalytic activity, as discussed in section 3.2.
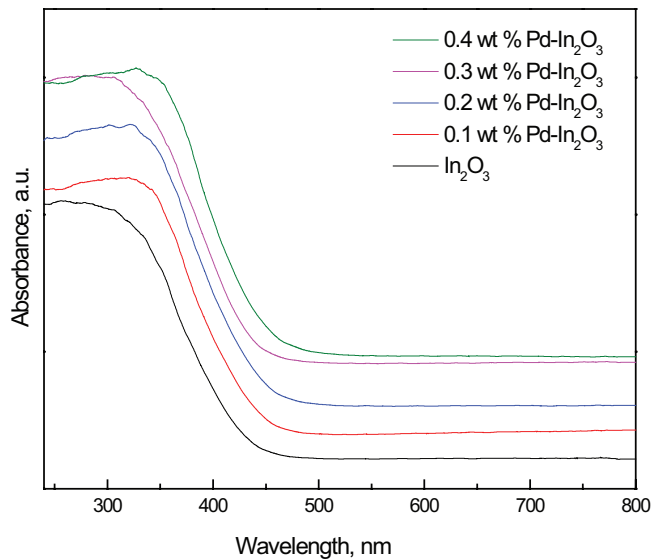
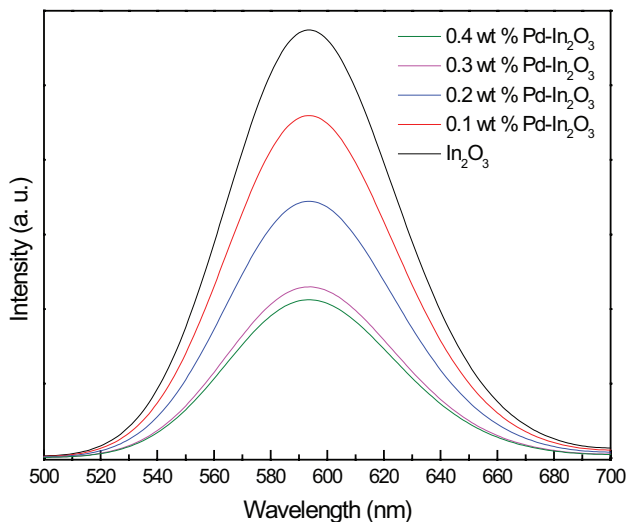Fig. 4. UV–Vis spectra of indium oxide and palladium-doped indium oxide nanocomposites.

Fig. 6. Effect of weight percentage of palladium on photocatalytic activity of indium oxide nanocomposites for degradation of atrazine.

Fig. 5. PL spectra of indium oxide and palladium-doped indium oxide nanocomposites.

3.2. Photocatalyst performance for atrazine degradation

Fig. 6 shows the photocatalytic degradation of atrazine using indium oxide and Pd-doped indium oxide nanocomposites. The results reveal that indium oxide can degrade 40% of the atrazine after 120 min, while degradation efficiencies after 120 min were 70%, 86% and 100% using 0.1 wt% Pd-In_2O_3, 0.2 wt% Pd-In_2O_3 and 0.3 wt% Pd-In_2O_3, respectively. Additionally, we noticed that 0.4 wt% Pd-In_2O_3 photocatalyst has photocatalytic activity relatively identical to that of the 0.3 wt% Pd-In_2O_3 photocatalyst. Therefore, photocatalytic efficiency of the In_2O_3 photocatalyst can be controlled by controlling the weight percentage of the doped palladium metal, which agrees with the published results [36].

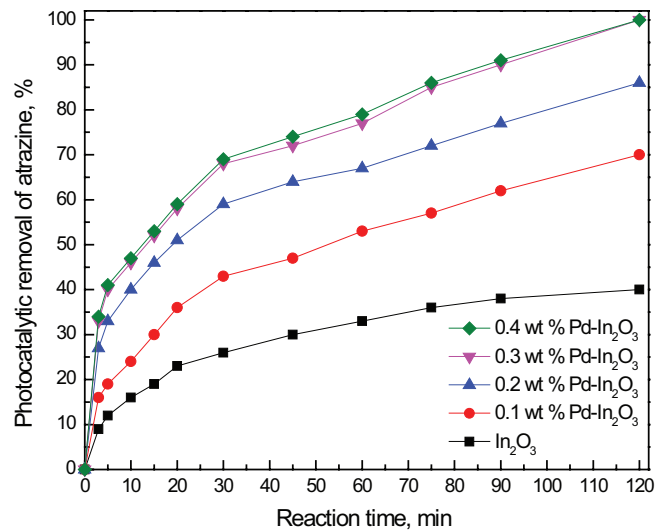The gases obtained from the atrazine degradation reaction were passed through a solution of sodium hydroxide with a 0.2 M concentration, and a solution of barium nitrate was added to the obtained materials; the obtained precipitate was identified by XRD. Fig. 7 shows the XRD results of the white precipitate. The results demonstrated that the phase of the obtained sample is barium carbonate. Therefore, atrazine is oxidized to carbon dioxide as one product of the photocatalytic oxidation process. Additionally, we detected chloride and nitrate ions, which were produced from the photocatalytic oxidation process of atrazine. Therefore, atrazine is completely degraded to Cl^-, NO_3^-, CO_2 and H_2O, which agrees with the published results [36].

Fig. 8 shows the dosing effect of 0.3 wt% palladium-doped indium oxide on atrazine degradation. The marks indicate that the degradation efficiency of 0.3 wt% palladium-doped indium oxide nanocomposite photocatalyst increased from 62% to 100% by increasing the dose of 0.3 wt% palladium-doped indium oxide nanocomposite from 0.5 to 1.0 g/L, respectively. The increasing dose from 1.0 to 1.5 g/L of 0.3 wt% palladium-doped indium oxide nanocomposite led to decreased reaction time for the complete degradation of atrazine from 120 to 75 min. The number of active sites available for the photocatalytic oxidation of atrazine was increased by increasing the dose of 0.3 wt% palladium-doped indium oxide. However, the reaction time was increased again from 75 to 120 min, and the photocatalytic activity was decreased from 100% to 81% by increasing the dose of 0.3 wt% palladium-doped indium oxide nanocomposite above 1.5 g/L. The penetration of light to the surface of the photocatalyst was decreased by the increased dose of the photocatalyst above the optimal dose, so the reaction time was decreased, while the photocatalytic activity was decreased, which agrees with published results [36].

Recycling and reuse of 0.3 wt% palladium-doped indium oxide photocatalyst for the degradation of atrazine is shown in Fig. 9. The results demonstrated that the 0.3 wt% palladium-doped indium oxide nanocomposite is a fivefold more stable photocatalyst for the degradation of atrazine, which agrees with published results [36].
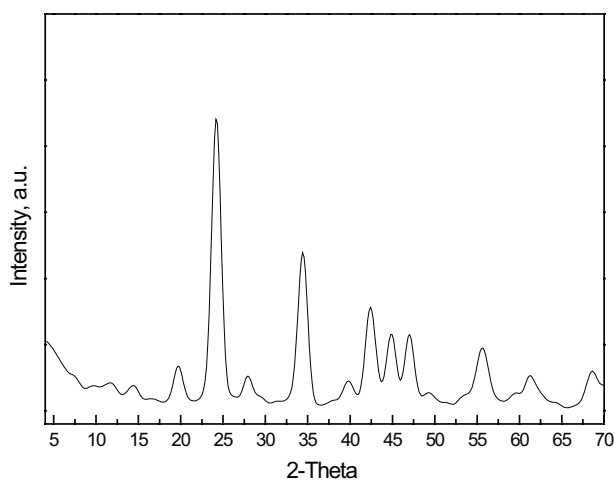
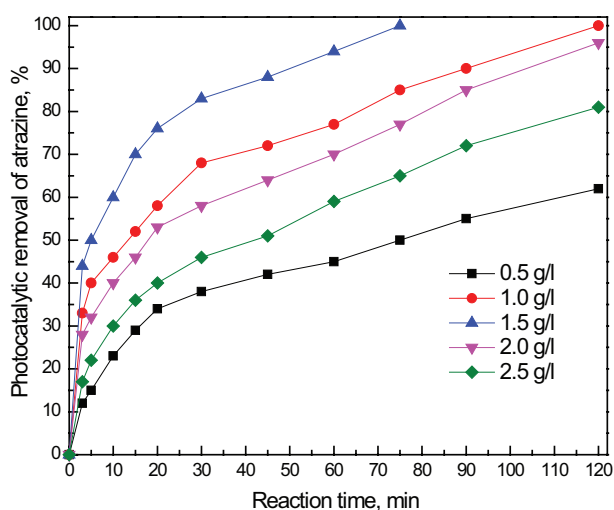Fig. 7. XRD patterns of the white precipitate.

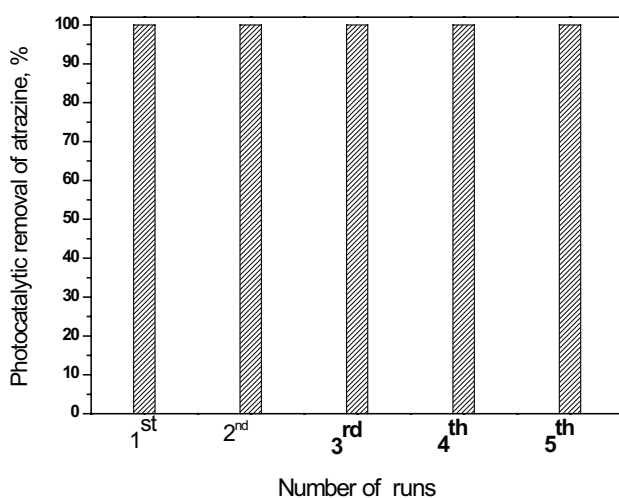Fig. 8. Effect of dose of 0.3 wt% palladium-doped indium oxide on degradation of atrazine.

Fig. 9. Recycling and reuse of 0.3 wt% palladium-doped indium oxide photocatalyst for degradation of atrazine.

4. Conclusions

A sol-gel method in the presence of TBAOH as a surfactant was used to prepare indium oxide and palladium-doped indium oxide nanocomposites. In_2O_3 and $Pd-In_2O_3$ nanocomposites were characterized using many tools. The results revealed that the activity and band gap of $Pd-In_2O_3$ nanocomposites can be controlled by the optimized weight percentage of palladium. $Pd-In_2O_3$ demonstrated a photocatalytic activity for the degradation of atrazine higher than that of indium oxide photocatalyst. The electron–hole recombination rate was decreased, and the absorption edge of indium oxide was shifted to a high wavelength by the addition of palladium to indium oxide. The 0.3 wt% palladium-doped indium oxide nanocomposite was a fivefold more stable photocatalyst during the degradation of atrazine.

References

[1] A. Alinsafi, F. Evenou, E.M. Abdulkarim, M.N. Pons, O. Zahraa, A. Benhammou, A. Yaacoubi, A. Nejmeddine, Treatment of textile industry wastewater by supported photocatalysis, Dyes Pigm., 74 (2007) 439–445.

[2] E. Eriksson, A. Baun, P.S. Mikkelsen, A. Ledin, Risk assessment of xenobiotics in stormwater discharged to Harrestrup Å, Denmark, Desalination, 215 (2007) 187–197.

[3] M. Neumann, R. Schulz, K. Schäfer, W. Müller, W. Mannheller, M. Liess. M. Neumann, R. Schulz, K. Schäfer, W. Müller, W. Mannheller, M. Liess, The significance of entry routes as point and non-point sources of pesticides in small streams, Water Res., 36 (2002) 835–842.

[4] C.S. Jacobsen, M.H. Hjelmsø, Agricultural soils, pesticides and microbial diversity, Curr. Opin. Biotechnol., 27 (2014) 15–20.

[5] X. Dong, L. Zhu, J. Wang, J. Wang, H. Xie, X. Hou, W. Jia, Effects of atrazine on cytochrome P450 enzymes of zebrafish, Chemosphere, 77 (2009) 404–412.

[6] R.M. Whyatt, R. Garfinkel, L.A. Hoepner, D. Holmes, M. Borjas, M.K. Williams, A. Reyes, V. Rauh, F.P. Perera, D.E. Camann, Within and between home variability in indoor-air insecticide levels during pregnancy among an inner-city Cohort from New York City, Environ. Health Perspect., 115 (2007) 383–389.

[7] S.M. Miller, C.W. Sweet, J.V. DePinto, K.C. Hornbuckle, Atrazine and nutrients in precipitation: results from the lake Michigan mass balance study, Environ. Sci. Technol., 34 (1999) 55–61.

[8] K.E. Banks, D.H. Hunter, D.J. Wachal, Chlorpyrifos in surface waters before and after a federally mandated ban, Environ. Int., 31 (2005) 351–356.

[9] A. Kaushik, H.R. Sharma, S. Jain, J. Dawra, C.P. Kaushik, Pesticide pollution of River Ghaggar in Haryana, India, Environ. Monit. Assess., 160 (2010) 61–69.

[10] S. Malato, J. Blanco, J. Cáceres, A.R. Fernández-Alba, A. Agüera, A. Rodríguez, Photocatalytic treatment of water-soluble pesticides by photo-Fenton and TiO_2 using solar energy, Catal. Today, 76 (2002) 209–220.

[11] S.C. Roy, O.K. Varghese, M. Paulose, C.A. Grimes, Toward solar fuels: photocatalytic conversion of carbon dioxide to hydrocarbons, ACS Nano, 4 (2010) 1259–1278.

[12] N. Atar, A. Olgun, F. Çolak, Thermodynamic, equilibrium and kinetic study of the biosorption of Basic Blue 41 using *Bacillus maceran*, Eng. Life Sci., 8 (2008) 499–506.

[13] V.K. Gupta, D. Mohan, S. Sharma, M. Sharma, Removal of basic dyes (Rhodamine B and methylene blue) from aqueous solutions using bagasse fly ash, Sep. Sci. Technol., 35 (2000) 2097–2113.

[14] N. Mohan, N. Balasubramanian, V. Subramanian, Electrochemical treatment of simulated textile effluent, Chem. Eng. Technol., 24 (2001) 749–753.

[15] J. Sojka-Ledakowicz, R. Zylla, Z. Mrozinska, K. Pazdzior, A. Klepacz-Smolka, S. Ledakowicz, Application of membrane

processes in closing of water cycle in a textile dye-house, Desalination, 250 (2010) 634–638.

[16] R. Velmurugan, M. Swaminathan, An efficient nanostructured ZnO for dye sensitized degradation of Reactive Red 120 dye under solar light, Sol. Energy Mater. Sol. Cells, 95 (2011) 942–950.

[17] D. Beydoun, R. Amal, G. Low, S. McEvoy, Role of nanoparticles in photocatalysis, J. Nanopart. Res., 1 (1999) 439–458.

[18] R. Esfandyarpour, H. Esfandyarpour, M. Javanmard, J.S. Harris, R.W. Davis, Label-free electronic probing of nucleic acids and proteins at the nanoscale using the nanoneedle biosensor, Biomicrofluidics, 7 (2013) 044114.

[19] R. Esfandyarpour, H. Esfandyarpour, J.S. Harris, R.W. Davis, Simulation and fabrication of a new novel 3D injectable biosensor for high throughput genomics and proteomics in a lab-on-a-chip device, Nanotechnology, 24 (2013) 465301.

[20] R. Esfandyarpour, H. Esfandyarpour, M. Javanmard, J.S. Harris, R.W. Davis, Microneedle biosensor: a method for direct label-free real time protein detection, Sens. Actuators B, 177 (2013) 848–855.

[21] P.A. Pekakis, N.P. Xekoukoulotakis, D. Mantzavinos, Treatment of Textile Dyehouse Wastewater by TiO_2 Photocatalysis, Water Res., 40 (2006) 1276–1286.

[22] Y. Bessekhouad, N. Chaoui, M. Trzpit, N. Ghazzal, D. Robert, J.V. Weber, UV–vis versus visible degradation of Acid Orange II in a coupled CdS/TiO_2 semiconductors suspension, J. Photochem. Photobiol. A, 183 (2006) 218–224.

[23] L. Pan, J.-J. Zou, S. Wang, Z.-F. Huang, X. Zhang, L. Wang, Enhancement of visible-light-induced photodegradation over hierarchical porous TiO_2 by nonmetal doping and water-mediated dye sensitization, Appl. Surf. Sci., 268 (2013) 252–258.

[24] J. Dostanic, B. Grbic, N. Radic, P. Stefanov, Z. Šaponjic, J. Buha, D. Mijin, Photodegradation of an azo pyridone dye using TiO_2 films prepared by the spray pyrolysis method, Chem. Eng. J., 180 (2012) 57–65.

[25] T. Kawahara, T. Ozawa, M. Iwasaki, H. Tada, S. Ito, Photocatalytic activity of rutile–anatase coupled TiO_2 particles prepared by a dissolution–reprecipitation method, J. Colloid Interface Sci., 267 (2003) 377–381.

[26] Q. Tian, W. Han, P. Liu, S. Lin, J. Zhuang, W. Yang, R. Qiu, β-In_2S_3 nanocrystals in Nafion membrane: facile synthesis and visible photocatalytic performance, Mater. Lett., 157 (2015) 127–130.

[27] Y. Guo, Z. Gong, P. Li, W. Zhang, B. Gao, Preparation, characterization and enhancement of the visible-light photocatalytic activity of In_2O_3/Na-bentonite composite, Ceram. Int., 42 (2016) 8850–8855.

[28] T.T. Tseng, J.Y. Uan, W.J. Tseng, Synthesis, microstructure, and photocatalysis of In_2O_3 hollow particles, Ceram. Int., 37 (2011) 1775–1780.

[29] J.B. Mu, B. Chen, M.Y. Zhang, Z.C. Guo, P. Zhang, Z.Y. Zhang, Y.Y. Sun, C.L. Shao, Y.C. Liu, Enhancement of the visible-light photocatalytic activity of In_2O_3–TiO_2 nanofiber heteroarchitectures, ACS Appl. Mater. Interfaces, 4 (2012) 424–430.

[30] Z.Y. Wang, B.B. Huang, Y. Dai, X.Y. Qin, X.Y. Zhang, P. Wang, H.X. Liu, J.X. Yu, Highly photocatalytic ZnO/In_2O_3 heteronanostructures synthesized by a coprecipitation method, J. Phys. Chem. C, 113 (2009) 4612–4617.

[31] S.K. Poznyak, D.V. Talapin, A.I. Kulak, Highly photocatalytic ZnO/In_2O_3 heteronanostructures synthesized by a coprecipitation method, J. Phys. Chem. B, 105 (2001) 4816–4823.

[32] K. Hara, K. Sayama, K. Arakawa, Semiconductor-sensitized solar cells based on nanocrystalline In_2S_3/In_2O_3 thin film electrodes, Sol. Energy Mater. Sol. Cells, 62 (2000) 441–447.

[33] D. Wang, Z.G. Zou, J.H. Ye, Photocatalytic water splitting with the Cr-doped $Ba_2In_2O_5$/In_2O_3 composite oxide semiconductors, Chem. Mater., 17 (2005) 3255–3261.

[34] Y.P. Sun, C.J. Murphy, K.R. Reyes-Gil, E. Reyes-García, J.P. Lilly, D. Raftery, Carbon-doped In_2O_3 films for photoelectrochemical hydrogen production, Int. J. Hydrogen Energy, 33 (2008) 5967–5974.

[35] N. Lu, C. Shao, X. Li, F. Miao, K. Wang, Y. Liu, A facile fabrication of nitrogen-doped electrospun In_2O_3 nanofibers with improved visible-light photocatalytic activity, Appl. Surf. Sci., 391 (2017) 668–676.

[36] R.M. Mohamed, Synthesis and characterization of AgCl@ graphitic carbon nitride hybrid materials for the photocatalytic degradation of atrazine, Ceram. Int., 41 (2015) 1197–1204.